

# Tunable Weyl Semi-metal and its Possible Realization in Optical Lattice

Xiao Kong,<sup>1</sup> Ying Liang,<sup>1</sup> and Su-Peng Kou<sup>1,\*</sup>

<sup>1</sup>*Department of Physics, Beijing Normal University.*

Weyl semimetal (WSM) is an exotic topological state in condensed matter physics. In this paper, based on a two-band cubic lattice model, we studied WSMs with a pair of tunable Weyl nodes. It is pointed out that there exist three types of WSMs with different tilt strengths: type-I WSM, type-II WSM and type-1.5 WSM. In particular, type-1.5 WSM has one type-I node and one type-II node. We studied chiral modes, surface Fermi arcs and quantum anomalous Hall effect in different types of WSMs. In addition, we give an experimental setup to realize the different types of WSMs based on timely technique.

**PACS numbers** 37.10.Jk, 72.90.+y, 67.85.Lm

Weyl semimetal (WSM) is a three-dimensional Graphene-like system with low-energy relativistic excitations[1–4]. In condensed matter physics, WSM was proposed to separate a single Dirac node into two Weyl nodes by breaking either time reversal symmetry or inversion symmetry. Thus, Weyl nodes always appear and disappear in pairs with opposite chiralities. For example, there are 12 pairs of Weyl nodes in the pyrochlore iridates  $A_2Ir_2O_7$  and in the TaAs. Recently, a new type of Weyl semimetal is proposed, which is called type-II Weyl semimetal (we denote it by WSM-II and traditional WSM by WSM-I)[5]. For WSM-II, the electron and hole pockets touch and the dispersions become anisotropic[6–8]. WSM-II was predicted in systems of  $Mo_xW_{1-x}Te_2$ [9], and then the surface Fermi arcs in  $MoTe_2$  were observed[10]. Due to its novel physics properties, such as chiral magnetic effect, negative magnetoresistance effect and surface Fermi arcs, WSM becomes hot topic in condensed matter physics[11–19]. Now, searching for materials of WSMs with few Weyl nodes is still an open problem.

The studies of ultracold atoms in optical lattices are extensively developed[20, 21]. Because of their precise control over the system parameters and defect-free properties, ultracold atoms in optical lattices provide an ideal platform to study many-body physics in condensed matters[22, 23]. Since the simulating magnetic fields (especially the non-Abelian ones) in ultra-cold atom gases was achieved, investigations on topological phases become an important issue. In Ref.[24], WSM-I was designed on optical lattices. However, WSM-II has not been simulated on optical lattices of ultracold atoms.

In this paper, based on an experimental setup in optical lattice for generating and freely controlling WSM, we realize different types of WSMs with a pair of tunable Weyl nodes. In particular, we realize a new region of WSM which contains one type-I node and one type-II node. We call it type-1.5 WSM (WSM-1.5). In this paper, we will show the physical properties for different types of WSMs and discuss how to realize them.

*Model Hamiltonian of generalized WSMs:* Our starting point is a two-band cubic lattice model for WSM-I[11], of which the Hamiltonian is written as

$$\begin{aligned}
 H_I = & \sum_i t_x (c_{i\uparrow}^\dagger c_{i+\hat{x}\downarrow} + c_{i\downarrow}^\dagger c_{i+\hat{x}\uparrow}) - t_y (c_{i\uparrow}^\dagger c_{i+\hat{y}\downarrow} \\
 & - c_{i\downarrow}^\dagger c_{i+\hat{y}\uparrow}) - \frac{m}{2} (c_{i\uparrow}^\dagger c_{i+\hat{y}\downarrow} + c_{i\downarrow}^\dagger c_{i+\hat{y}\uparrow}) \\
 & - e^{i\pi/2} t_z (c_{i\uparrow}^\dagger c_{i+\hat{z}\uparrow} - c_{i\downarrow}^\dagger c_{i+\hat{z}\downarrow}) \\
 & - \frac{m}{2} (c_{i\uparrow}^\dagger c_{i+\hat{z}\downarrow} + c_{i\downarrow}^\dagger c_{i+\hat{z}\uparrow}) + h.c. \\
 & + 2(m - \cos k_0) (c_{i\uparrow}^\dagger c_{i\downarrow} + c_{i\downarrow}^\dagger c_{i\uparrow}), \quad (1)
 \end{aligned}$$

where  $i$  denotes the lattice site,  $c$  and  $c^\dagger$  are annihilation and creation operators,  $\hat{x}$ ,  $\hat{y}$  and  $\hat{z}$  represent the nearest-neighbor vectors along  $x$ ,  $y$  and  $z$  axes and  $h.c.$  is short of hermitian conjugate.  $t_{x,y,z}$  are hopping parameters and  $m$  is the strength of on-site "external field".  $k_0$  denotes a constant wave vector.  $\uparrow$  and  $\downarrow$  are pseudo spin degrees of freedom. By Fourier transformation, Eq.1 turns into  $H_I = \sum_k c_k^\dagger \mathbf{h}_I(k) c_k$ , where

$$\begin{aligned}
 \mathbf{h}_I(k) = & [2t_x (\cos k_x - \cos k_0) \\
 & + m(2 - \cos k_y - \cos k_z)] \cdot \sigma_x \\
 & + 2t_y \sin k_y \cdot \sigma_y + 2t_z \sin k_z \cdot \sigma_z, \quad (2)
 \end{aligned}$$

where  $\sigma_{x,y,z}$  represent Pauli matrices. For the case of  $m > 2t_x(1 + \cos k_0)$ , this model has two Weyl nodes at  $\mathbf{K}_+ = (k_0, 0, 0)$  and  $\mathbf{K}_- = (-k_0, 0, 0)$ , with Fermi velocities  $\mathbf{v}_+ = (-2t_x \sin k_0, 2t_y, 2t_z)$  and  $\mathbf{v}_- = (2t_x \sin k_0, 2t_y, 2t_z)$ . The low-energy Hamiltonians near nodes can be written as  $\mathbf{h}_I(k) \simeq \sum_{n=+,-,i} v_{n,i} k_i \cdot \sigma_i$ . The chiralities of nodes are  $\text{sgn}(\prod_i v_{n,i})$  which could be  $\pm 1$ .

Based on the WSM-I Hamiltonian in Eq.2, we obtain a generalized WSM by tilting the two nodes. In general, to arbitrarily tune the Weyl nodes, we may add the following terms  $\mathbf{h}_{\text{tilt}} = \mathbf{h}_{ox} + \mathbf{h}_{sx} + \mathbf{h}_{sy} + \mathbf{h}_{sz} + \mathbf{h}_{oy} + \mathbf{h}_{oz}$

\*Electronic address: [spkou@bnu.edu.cn](mailto:spkou@bnu.edu.cn)

where

$$\begin{aligned}
\mathbf{h}_{ox} &= \sum_i v_{ox} (c_{i\uparrow}^\dagger c_{i+\hat{x}\uparrow} + c_{i\downarrow}^\dagger c_{i+\hat{x}\downarrow}) + h.c. \\
&\quad - 2v_{ox} \cos k_0 (c_{i\uparrow}^\dagger c_{i\uparrow} + c_{i\downarrow}^\dagger c_{i\downarrow}), \\
\mathbf{h}_{sx} &= \sum_i e^{i\pi/2} v_{sx} (c_{i\uparrow}^\dagger c_{i+\hat{x}\uparrow} + c_{i\downarrow}^\dagger c_{i+\hat{x}\downarrow}) + h.c. \\
&\quad - 2v_{sx} \sin k_0 (c_{i\uparrow}^\dagger c_{i\uparrow} + c_{i\downarrow}^\dagger c_{i\downarrow}), \\
\mathbf{h}_{sy/sz} &= \sum_i e^{i\pi/2} v_{sy/sz} (c_{i\uparrow}^\dagger c_{i+\hat{y}/\hat{z}\uparrow} + c_{i\downarrow}^\dagger c_{i+\hat{y}/\hat{z}\downarrow}) + h.c., \\
\mathbf{h}_{oy/oz} &= \sum_i v_{oy/oz} (c_{i\uparrow}^\dagger c_{i+\hat{y}/\hat{z}+\hat{x}\uparrow} + c_{i\downarrow}^\dagger c_{i+\hat{y}/\hat{z}+\hat{x}\downarrow}) \\
&\quad - \sum_i v_{oy/oz} (c_{i\uparrow}^\dagger c_{i+\hat{y}/\hat{z}-\hat{x}\uparrow} + c_{i\downarrow}^\dagger c_{i+\hat{y}/\hat{z}-\hat{x}\downarrow}) + h.c.,
\end{aligned} \tag{3}$$

where  $\mathbf{I}$  is  $2 \times 2$  identity matrix. Thus, the total low-energy effective model becomes

$$\begin{aligned}
\mathbf{h}_{\text{total}}(k) &= \mathbf{h}_I(k) + \mathbf{h}_{\text{tilt}} \simeq v_F [\alpha_\pm \mathbf{n}_\pm \cdot (\mathbf{k} - \mathbf{K}_\pm) \mathbf{I} \\
&\quad \pm (\mathbf{k} - \mathbf{K}_\pm) \cdot \boldsymbol{\sigma} \pm \frac{b_\pm}{2} \mathbf{I}],
\end{aligned} \tag{4}$$

where  $\mathbf{n}_\pm$  is tilt strength vector which defines tilt direction of nodes,  $\alpha_\pm$  is tilt strength, a parameter describing amplitude of tilt and  $b_\pm$  the chemical potential of nodes.

We have four free parameters that describe the low energy physics of a node,  $\mathbf{K}_+$  (or  $\mathbf{K}_-$ ),  $\mathbf{n}_+$  (or  $\mathbf{n}_-$ ),  $\alpha_+$  (or  $\alpha_-$ ),  $b_+$  ( $b_-$ ). A detailed calculations are given in supplementary-materials. For a given Weyl node, there exists two phases: in the region of  $\alpha_\pm < 1$ , the (tilting) Weyl node belongs to type-I; in the region of  $\alpha_\pm > 1$ , the (tilting) Weyl node belongs to type-II, in which the electron pocket and hole pocket contact each other. As a result, there exist three types of WSMs: for the case of  $\alpha_+ < 1$  and  $\alpha_- < 1$  we call the WSM to be type-I WSM (WSM-I); for the case of  $\alpha_+ > 1$  and  $\alpha_- > 1$ , we call it type-II WSM (WSM-II); for the case of  $\alpha_+ > 1$  and  $\alpha_- < 1$  and the case of  $\alpha_+ < 1$  and  $\alpha_- > 1$ , we call it type-1.5 WSM (WSM-1.5). We show the phase diagram and dispersions of WSMs in Fig.1.

*Surface Fermi arcs for different types of WSMs:* In our model, nodes are separated along  $\hat{x}$ -direction. Fermi arcs appear except for the projection along  $\hat{x}$ -direction. For WSM-I with  $\alpha_\pm = 0$ , Fermi arcs on opposite surfaces have the same dispersion. See the results in Fig.2(c). To study the surface states in a WSM system, we cut the 3-dimensional system to parallel 2-dimensional (2D) systems piece by piece along  $\hat{x}$ -direction and get a 2D topological insulator with  $k_0 > k_x > -k_0$ , of which the surface states have the effective Hamiltonian as  $\mathbf{h}_{\text{surface}} = 2t_y \sin k_y \sigma_z$ ,  $k_x \in (-k_0, k_0)$  where  $\sigma_z$  is the pseudo-spin operator of surfaces.

We then study the surface Fermi arcs in WSMs with  $\alpha_\pm \neq 0$ . Firstly, we study the tilting effect on surface states along  $\hat{x}$ -direction (the tilt direction of node

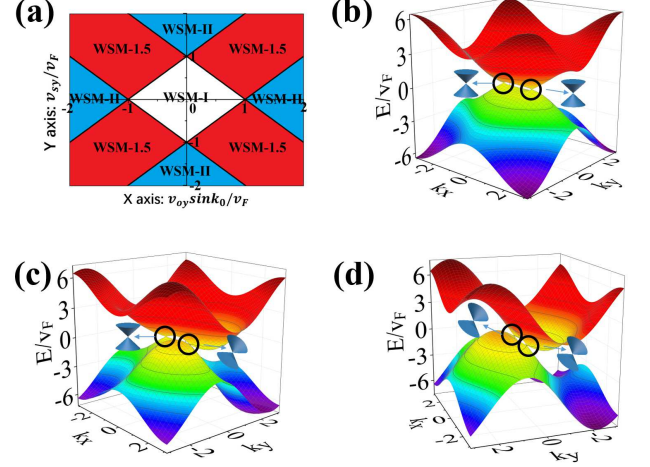


FIG. 1: (color online) Illustration of different WSMs: (a) phase diagram of parameters  $v_{oy}$  and  $v_{sy}$ ; (b) WSM-I without tilts of nodes; (c) WSM-1.5 with one type-I node and one type-II node, parameters are set as  $\mathbf{n}_+ = (0, 1, 0)$ ,  $\alpha_+ = -1.2$  and  $\alpha_- = 0$ ; (d) WSM-II with same tilts perpendicular to the node-separation, parameters are set as  $\mathbf{n}_+ = \mathbf{n}_- = (0, 1, 0)$  and  $\alpha_+ = \alpha_- = -1.2$ .

$(k_0, 0, 0)$  is set to be  $\mathbf{n}_+ = (1, 0, 0)$ ). Due to the existence of an additional term  $\mathbf{h}_{\text{tilt}} = v_F \alpha_+ l' \cdot \mathbf{I}$  on each  $k_y$ - $k_z$  plane where  $l' = k_x - k_0$ , the effective Hamiltonian of the surface states  $\mathbf{h}_{\text{surface}}$  has an energy shift that is proportional to  $l'$ . As a result, the shape of Fermi arcs changes. However, the situation changes when we study the tilting effect on surface states along  $\hat{y}$ -direction. Now, the tilt direction of node  $(k_0, 0, 0)$  becomes  $\mathbf{n}_+ = (0, 1, 0)$ . Because the translation invariance along  $\hat{y}$ -direction is not broken, we can easily derive the surface effective Hamiltonian by the method in Ref.[25] and obtain  $\mathbf{h}_{\text{surface}} = v_F k_y \sigma_z + v_F \alpha_+ k_y \mathbf{I}$ . As a result, the dispersion of surface states near nodes are tilted and shows similar behaviour as those in bulk. For example, in a WSM-II, the surface states are also in "type-II". See the illustration in Fig.2.

*Chiral modes of different types of WSMs in magnetic field:* When applying magnetic field  $B\hat{x}$  to WSM-I system, there are two chiral modes: one comes from the zeroth Landau level near node  $k_0$ , the other comes from the zeroth Landau level near node  $-k_0$ . As a result, WSM-I behaves chiral anomaly such as negative magnetoresistance effect and chiral magnetic effect[14, 19, 26].

We then study the chiral modes in WSMs with  $\alpha_\pm \neq 0$ . According to Ref.[7], when a magnetic field perpendicular to  $\mathbf{n}$  is applying to the system, the Landau levels in WSM-IIs are collapsing, the system then have no chiral modes[5]. Thus, when magnetic field is perpendicular to tilting direction, no chiral mode appears and the system doesn't behave chiral anomaly. For the case of WSM-1.5,

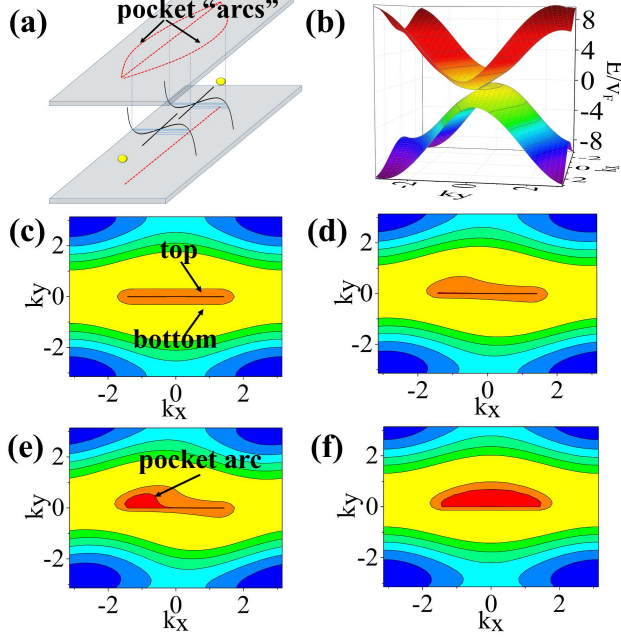


FIG. 2: (color online) Surface Fermi arcs. (a) A scheme of Fermi arcs in WSM-II, surface states are tilted so that their electron and hole pockets also cross Fermi surface. There is an additional Fermi circle appears in one surface. We split them into two arcs and call them pocket arcs. The yellow balls are Weyl points and the red dash lines are Fermi arcs; (b) Type-II surface states; (c)-(f) show energy contours of surface state. The edge of orange area is cut by  $E = -0.3v_F$  and the edge of red area is cut by  $E = -0.015$ , respectively. The parameters are  $\alpha_+ = \alpha_- = 0$  for (c),  $\alpha_+ = 0, \alpha_- = 0.5$  for (d),  $\alpha_+ = 0, \alpha_- = 1.2$  for (e) and  $\alpha_+ = \alpha_- = 1.2$  for (f). The tilting direction is  $\mathbf{n}_+ = \mathbf{n}_- = (0, 1, 0)$ .

one node is type-I and the other is type-II. In Fig.3, we calculate the energy spectrum of WSM-1.5 in magnetic field. Obviously, there is a linear chiral mode near the type-I node  $(-k_0, 0, 0)$  and the bands near the type-II node  $(k_0, 0, 0)$  are gapped.

In addition, we calculate the Hall conductance in different WSMs and show the results in Fig.3(d). For WSM-I with zero chemical potential, there exists quantum anomalous Hall effect and the Hall conductance is  $\sigma_{yz} = \frac{e^2 k_0}{2\pi^2 \hbar}$  (that corresponds to the platform in Fig.3(d)). We then tilt the WSM with zero chemical potential into WSM-II and WSM-1.5. Due to finite density at Fermi surface, the Hall conductance will not be a constant and decrease with tilt strength.

*Experimental setup for different types of WSMs in optical lattice:* Designing an experimental setup in optical lattice, which possesses both tunable anisotropic properties and intact band structure, is impending for the studies on WSM-II and WSM-1.5. In this part, we use

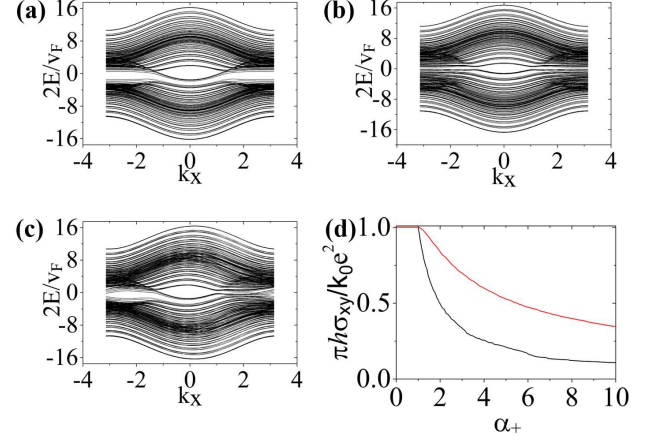


FIG. 3: (color online) (a) Dispersion of WSM-I in a magnetic field along  $\hat{x}$ . There are two chiral modes near Fermi surface  $E = 0$ ; (b) Dispersion of WSM-II with  $\mathbf{n}_+ = \mathbf{n}_- = (0, 1, 0)$  and  $\alpha_+ = \alpha_- = 1.2$  in a magnetic field along  $\hat{x}$ . There are no chiral mode and the spectrum is gapped; (c) Dispersion of WSM-1.5 with  $\alpha_- = 0$ ,  $\mathbf{n}_+ = (0, 1, 0)$  and  $\alpha_+ = 1.2$  in a magnetic field along  $\hat{x}$ . There exists a chiral mode; (d) Hall conductivity in WSMs. The black line is the result for the case of  $\mathbf{n}_+ = \mathbf{n}_- = (0, 1, 0)$  and  $\alpha_+ = \alpha_- = \alpha$ . The red line is the result for the case of  $\mathbf{n}_+ = (0, 1, 0)$ ,  $\alpha_+ = \alpha$  and  $\alpha_- = 0$ .

Fermi atom gases with two long-life hyperfine levels to simulate different types of WSMs[27].

At the beginning, we construct the optical lattice by standing waves:  $V(x, y, z) = -V_0 \sum_{i=x,y,z} [\cos^2(qi) - V'_0 \cos^2(2qi)]$ , where  $x, y, z$  denote the different directions,  $q = \frac{2\pi}{\lambda}$  is the recoiling momentum and  $V_0$  and  $V'_0$  are positive potential amplitudes. The standing waves have a cubic array of minima separated by second minima sites. The atoms are trapped in the standing waves and we can use the Wannier functions  $\omega_{n,\mathbf{R}}(\mathbf{r})$  to describe the states on each site, where  $n$  is band index,  $\mathbf{R}$  the location of site and  $\mathbf{r}$  the displacement from  $\mathbf{R}$ . Let us consider  $^{40}\text{K}$  atoms in the present of a uniform magnetic field  $\mathcal{B}$ , and employ the two hyperfine manifolds of ground states:  $F = 9/2$  and  $F = 7/2$ . The energies are  $E_{9/2,m_F} = g_F \mu_B \mathcal{B} m_F$  and  $E_{7/2,m_F} = \Delta_{HF} - g_F \mu_B \mathcal{B} m_F$ , where  $g_F$  is the hyperfine Landé factor,  $\mu_B$  the Bohr magneton and  $m_F$  the projection along magnetic field.

Now, setting large potential amplitudes, we get a cubic optical lattice with atoms trapped in minima and second minima sites without any hopping. To realize the desired hopping terms, we apply four Raman laser beams to the system. We take the following term as an example:  $-t_x e^{i\phi_a} c_a^\dagger \sigma_x c_{a+\hat{x}} + h.c.$ , where  $t_x$  is the real hopping strength,  $a$  the site of optical lattice (that is a local minimum),  $\hat{x}$  the vector from a site to its nearest site along  $x$  and  $\phi_a$  the phase of hopping;  $c_a$  is annihilation operators with (pseudo) spins  $c_a = (c_{a\uparrow}, c_{a\downarrow})^T$  and  $\sigma_x$  the Pauli



matrix. This term corresponds to the first hopping term in Eq.1 for the case of  $\phi_a = 2\pi * \text{integer}$ .

We then employ a pair of Raman laser beams which couple a ground state to an auxiliary state with net momentum  $\mathbf{q}$  and frequency  $\omega_1$ , and another pair of  $\mathbf{q}$ ,  $\omega_2$  couple auxiliary state to another ground state. For the Wannier state  $|F = 9/2, m_F = 9/2\rangle_a$  on site  $a$  and  $|F = 9/2, m_F = 7/2\rangle_{a+\hat{x}}$  on site  $a + \hat{x}$ , we have the energies of them  $E_{a,9/2} = 9g_F\mu_B\mathcal{B}/2$ ,  $E_{a+\hat{x},7/2} = 7g_F\mu_B\mathcal{B}/2$ . The auxiliary state  $|F = 7/2, m_F = 7/2\rangle_{a+\hat{x}/2}$  on second minimum site has energy  $E_{a+\hat{x}/2,7/2} = \Delta_{HF} + V_0 - 7g_F\mu_B\mathcal{B}/2$ . We set the frequency difference  $\omega_2 - \omega_1 \approx g_F\mu_B\mathcal{B}$  so that the ground dressed states are nearly degenerate. Moreover, for the detuning  $\delta$  to be  $\delta = \Delta_{HF} + V_0 - 7g_F\mu_B\mathcal{B} - \omega_2$ , the excited dressed states have higher energies and can be treated as auxiliary states. By adiabatic eliminating the auxiliary states, we could derive an effective Hamiltonian as  $H_{eff} = -\frac{|\Omega|^2}{\delta}e^{2i\mathbf{q}\cdot\mathbf{a}}c_{a,\uparrow}^\dagger c_{a+\hat{x},\downarrow}$ , where  $\Omega$  is the strength of Raman coupling between the ground states and the auxiliary state,  $\mathbf{a}$  denotes the position of site  $a$ . The spin indices  $\uparrow$  for hyperfine levels represents the state  $|F = 9/2, m_F = 9/2\rangle$  and  $\downarrow$  for  $|F = 9/2, m_F = 7/2\rangle$ . By considering another two pairs of Raman lasers that couple the ground states to the auxiliary state  $|F = 7/2, m_F = 5/2\rangle_{a+\hat{x}/2}$ , we may derive the following coupling  $H_{eff} = -\frac{|\Omega|^2}{\delta}e^{2i\mathbf{q}\cdot\mathbf{a}}c_{a,\downarrow}^\dagger c_{a+\hat{x},\uparrow}$ . As a result, the effective Hamiltonian  $-t_x e^{i\phi_a} c_{a,\downarrow}^\dagger c_{a+\hat{x},\uparrow} + h.c.$  is obtained after fixing the parameters  $t_x = \frac{|\Omega|^2}{\delta}$  and  $\phi_a = e^{i2\mathbf{q}\cdot\mathbf{a}}$ . Therefore, the lattice model of WSM-II in Eq.4 could be realized by similar method step-by-step. For example, the next-nearest-neighbor hopping could be realized by employing auxiliary states on second minima sites in the center of four minima sites, which is shown in Fig.4.

However, if we consider the next-nearest neighbor hopping (for example,  $\mathbf{h}_{oy}$ ) by employing two pairs of Raman lasers with the momentum difference  $\Delta\mathbf{q} = (\frac{\pi}{2|\hat{x}|}, \frac{\pi}{2|\hat{x}|}, 0)$ , the lasers could also induce an additional hopping term along  $x$  and  $y$  directions with  $\pi$  flux per plaquette. To avoid the interferences between different Raman processes, we apply an anisotropy gradient potential on the system. If the potential on site  $a$  is 0, it on  $a + \hat{x}(\hat{y}, \hat{z})$  is  $\Delta_x(\Delta_y, \Delta_z)$  and  $\Delta_i \neq \Delta_j$  if  $i \neq j$ . Thus, two pairs of Raman lasers would have frequency difference  $\omega_2 - \omega_1 = (\Delta_x + \Delta_y(\Delta_z))$  for hopping between same hyperfine state  $|F = 9/2, m_F\rangle_a$  and  $|F = 9/2, m_F\rangle_{a+\hat{x}+\hat{y}(\hat{z})}$  on  $x-y(z)$  plane. Frequency differences of other Raman lasers are also modified to match the gradient. In the end, after adding the gradient magnetic field, a tunable WSM-II system is designed on optical lattice. The second minima sites (or the light potential  $V'_0$ ) is not necessary for simulating a WSM, so the setup could be simplified as we only need one pair of Raman lasers to induce a hopping term. However, we prefer the second minima sites to exist because it gives an additional parameter  $\delta$

to simulate more complicate phenomena.

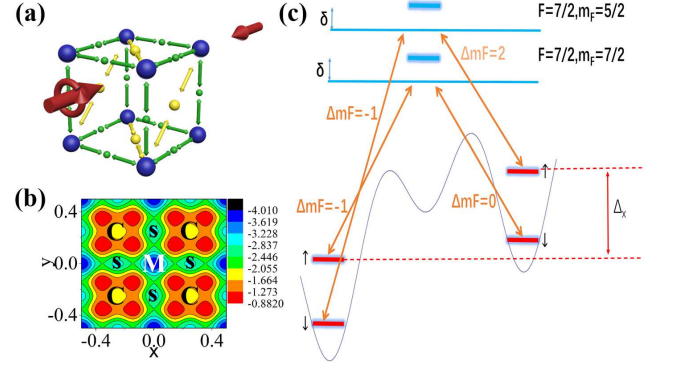


FIG. 4: (color online) (a) An illustration of our purpose to realize WSMs. Blue balls represent minima sites and green and yellow balls represent second minima sites. Double sided arrows denote the Raman couplings. Red arrows denote Raman lasers for a Raman coupling with  $\Delta m_F = -1$ , of which a circle arrow marks an unit of angular momentum carried by a  $\sigma$  laser; (b) The lattice potential for all hyperfine states without gradient potential.  $\mathbf{M}$  denote minima sites,  $\mathbf{S}$  denotes second minima sites and  $\mathbf{C}$  center second minima sites; (c) A scheme of realizing spin-flipping terms in the present of a gradient potential.

In the end of this paper, we give a summary. We proposed a tunable two-band lattice model in optical lattice which corresponds to a WSM system. There exist three types of WSMs with different tilt strengths: WSM-I, WSM-II and WSM-1.5. We studied chiral modes, surface Fermi arcs and quantum anomalous Hall effect in different types of WSMs. In a WSM-1.5 only one chiral mode occurs, which may imply novel chiral anomaly in this system. The Dirac cone of surface states are also tilted when we tilt nodes along certain directions ( $\hat{y}$  or  $\hat{z}$  in our model) in bulk. In addition, we designed an experimental setup for different types of WSMs in optical lattice that provides a platform for further studies on WSM systems.

\* \* \*

This work is supported by National Basic Research Program of China (973 Program) under the grant No. 2012CB921704 and NSFC Grant No. 11174035, 11474025, 11404090, We also acknowledge the support from the Fundamental Research Funds for the Center Universities with No. 2014KJJC26 (Y. Liang).

After we finished this work, we found the concept of type-1.5 WSM also to be proposed as hybrid WSM in Ref.[28] a few days ago. Our works are independent to each other.

- 
- [1] X. Wan, A.M. Turner, A. Vishwanath, S.Y. Savrasov, *Physical Review B* **83**, 205101 (2011).
  - [2] Shin-Ming Huang, et al., *Nature Communications* **6**, 7373 (2015).
  - [3] B. Q. Lv, et al., *Physical Review X* **5**, 031013 (2015).
  - [4] B. Q. Lv, et al., *Nature Physics* **11**, 724 (2015).
  - [5] Alexey A. Soluyanov, et al., *Nature* **527**, 495 (2015).
  - [6] A. A. Zyuzin, et al., arXiv: 1601.00890 (2016).
  - [7] Zhiming Yu, et al., arXiv: 1604.04030 (2016).
  - [8] M. Udagawa, et al., arXiv: 1604. 08457 (2016).
  - [9] Tay-Rong Chang, et al., *Nature Communications* **7** 10639 (2016).
  - [10] N. Xu, et al., arXiv: 1604. 02116 (2016).
  - [11] Kai-Yu Yang, et al., *Physical Review B* **84**, 075129 (2011).
  - [12] Xiaochun Huang, et al., *Physical Review X* **5**, 031023 (2015).
  - [13] Pallab Goswami, et al., arXiv: 1311.1506 (2013).
  - [14] A. A. Zyuzin, A. A. Burkov, *Physical Review B* **86** 115133 (2012).
  - [15] D. T. Son, B. Z. Spivak, *Physical Review B* **88** 104412 (2013).
  - [16] Dmitri E. Kharzeev, H. U. Yee, *Physical Review B* **88** 115119 (2013).
  - [17] Pallab Goswami, et al., *Physical Review B* **88** 245107 (2013).
  - [18] M. M. Vazifeh, M. Franz, *Physical Review Letters* **111** 027201 (2013).
  - [19] Chao-Xing Liu, et al., *Physical Review B* **87** 235306 (2013).
  - [20] M. Greiner, et al., *Nature*, **415**, 39 (2002).
  - [21] D. Jaksch, C. Bruder, J. I. Cirac, C. W. Gardiner, P. Zoller, *Physical. Review. Letters.* **81**, 3108 (1998).
  - [22] Maciej Lewenstein, et al., *Advances in Physics*, **56**, 243 (2007).
  - [23] I. Bloch, et al., *Rev. Mod. Phys.* **80**, 885 (2008).
  - [24] Tena Dubček, et al., *Physical Review Letters* **114**, 225301 (2015).
  - [25] Shun-Qing Shen, *Topological Insulators*, Springer (2012)
  - [26] Pavan Hosur, et al., *Comptes Rendus Physique* **14**, 857 (2013).
  - [27] Leonardo Mazza, et al., *New Journal of Physics* **14**, 015007 (2012).
  - [28] Fei-Ye Li, et al., arXiv:1607, 08474 (2016).